

Dynamical Conductivity Across The Disorder-Tuned Superconductor-Insulator Transition

Mason Swanson¹, Yen Lee Loh², Mohit Randeria¹, and Nandini Trivedi¹

(1) *Department of Physics, The Ohio State University, Columbus, OH 43210, USA and*

(2) *Department of Physics and Astrophysics, University of North Dakota, Grand Forks, ND 58202, USA*

(Dated: April 2, 2022)

A quantum phase transition is a dramatic event marked by large spatial and temporal fluctuations, where one phase of matter with its ground state and tower of excitations reorganizes into a completely different phase. We provide new insight into the disorder-driven superconductor-insulator transition (SIT) in two dimensions, a problem of great theoretical and experimental interest, with the dynamical conductivity $\sigma(\omega)$ and the bosonic (pair) spectral function $P(\omega)$ calculated from quantum Monte Carlo simulations. We identify characteristic energy scales in the superconducting and insulating phases that vanish at the transition due to enhanced quantum fluctuations, despite the persistence of a robust fermionic gap across the SIT. Disorder leads to enhanced absorption in $\sigma(\omega)$ at low frequencies compared to the SIT in a clean system. Disorder also expands the quantum critical region, due to a change in the universality class, with an underlying $T = 0$ critical point with a finite low-frequency conductivity.

The interplay of superconductivity and localization has proven to be a rich and intriguing problem, especially in two dimensions^{1–7}. Both paradigms stand on the shoulders of giants – the BCS theory of superconductivity and the Anderson theory of localization. Yet, when the combined effects of superconductivity and disorder are considered, both paradigms break down, even for s-wave superconductors.

It has been shown^{8–10} in model fermionic Hamiltonians with attraction between electrons and disorder arising from random potentials, that the single-particle density of states continues to show a hard gap across the disorder-driven quantum phase transition and that pairs continue to survive into the insulating state. The superconducting transition temperature T_c , however, does decrease with increasing disorder and vanishes at a critical disorder signaling a superconductor-insulator transition (SIT). These theoretical predictions are supported by scanning tunneling spectroscopy experiments^{11–14} and by magnetoresistance oscillations⁶ in disordered thin films.

Recent conductivity measurements at frequencies well within the superconducting gap (0–20 GHz)^{15–20} have observed low-frequency features that cannot be accounted for by pair-breaking mechanisms. A theoretical understanding of the low-frequency dynamical conductivity is vital for understanding the role of fluctuations and for guiding future experiments that probe the SIT.

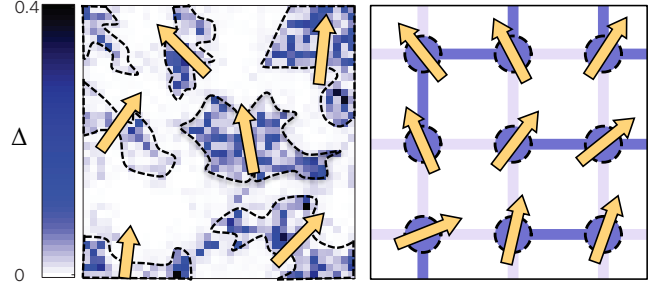


FIG. 1. The emergent inhomogeneity of the local pairing amplitude $\Delta(\mathbf{r})$ in a disordered superconductor in the left panel and the robustness of the single particle gap^{8–10} across the SIT suggests an effective low-energy description in terms of a disordered quantum XY model shown on the right. The quantum phase transition occurs when long range phase coherence is lost between weakly connected “superconducting islands” tuned by the ratio E_c/E_J of charging energy to Josephson coupling as well as by disorder, modeled by removing a fraction p of the Josephson bonds.

The robustness of the single-particle gap across the SIT suggests that the low-energy physics near the SIT can be described by an effective “bosonic” Hamiltonian, the disordered quantum XY model, where the relevant degrees of freedom are the phases of the local superconducting order parameter. This model is also relevant for ultracold atomic gases in optical lattices where the transition is tuned by changing the tunneling of bosons compared to their on-site repulsion^{21–24}. More recently, it has also become possible to include disorder in optical lattices using speckle patterns. By increasing the strength of the disorder potential it could be possible to drive quantum phase transitions from a superfluid to a Bose glass^{25–28}; our results are also relevant for such experiments.

We map the quantum (2+1)D XY Hamiltonian to an anisotropic classical 3D XY model^{29–31} and simulate the model using Monte Carlo methods. We focus on the behavior of two dynamical quantities of fundamental significance, the conductivity $\sigma(\omega)$ and the boson (“pair”) spectral function $P(\omega)$ obtained by analytic continuation from imaginary time using the maximum entropy method supplemented by sum rules. Disorder is introduced into the quantum model by breaking bonds (“Josephson couplings”) on a 2D square lattice with a probability p . We compare the results of the disorder-driven SIT with the clean system^{29,32}, where the SIT is tuned by E_c/E_J , the charging energy relative to the Josephson coupling.

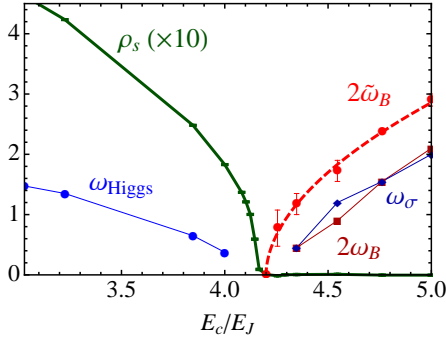


FIG. 2. Energy scales, in units of E_J , as a function of the control parameter E_c/E_J in the clean system. From the SC side, the superfluid stiffness ρ_s and the Higgs “mass” ω_{Higgs} , and from the insulating side, the optical conductivity threshold ω_σ and the boson energy scales ω_B and $\tilde{\omega}_B$, vanish at the transition creating a fan-shaped region where quantum critical fluctuations dominate.

Our main results are as follows.

- (1) The conductivity $\text{Re } \sigma(\omega)$ in the clean superconductor shows absorption above a threshold ω_{Higgs} that can be associated with the scale of the Higgs (amplitude) mode. As we approach the SIT from the superconducting (SC) side, both the superfluid stiffness ρ_s and the Higgs scale ω_{Higgs} go soft and vanish at the SIT, even though the fermionic energy gap remains finite across the transition.
- (2) In the insulating state of the clean system, we find a threshold ω_σ for absorption in $\text{Re } \sigma(\omega)$ and show that it is twice the gap ω_B in the bosonic spectral function $\text{Im } P(\omega)/\omega$. We show that both these scales go soft on approaching the SIT from the insulating side. Furthermore, in the insulator, $\text{Im } \sigma(\omega)$ becomes negative at low frequencies, indicating “capacitive” response.
- (3) The low-frequency spectral weight in $\text{Re } \sigma(\omega)$ for the disordered system is greatly enhanced relative to its clean counterpart, so that there is no clear optical gap in the vicinity of the SIT, despite the existence of a non-zero fermionic energy gap. We find that enhanced quantum phase fluctuations and rare regions generate low-frequency spectral weight for ω well below the clean ω_{Higgs} scale in the SC state, and well below the clean $\omega_\sigma = 2\omega_B$ scale on the insulating side.
- (4) The spectral function $\text{Im } P(\omega)/\omega$ has a characteristic peak in the insulator, whose energy $\tilde{\omega}_B$ is a measure of the inverse coherence time scale for bosonic (pair) excitations. The vanishing of the superfluid stiffness ρ_s on the SC side and the vanishing of $\tilde{\omega}_B$ from the insulating side are shown to demarcate the quantum critical regime at the SIT for both the clean and the disordered system.
- (5) The low-frequency conductivity σ^* in the quantum critical regime between the SC and the insulator can be estimated meaningfully from the integrated spectral weight over a frequency range of the order of the temperature (see Eq. 2). We find $\sigma^* \simeq 0.5(4e^2/h)$ at the disorder-driven SIT in comparison to $\sigma^* \simeq 0.4(4e^2/h)$ at the SIT in the pure system, in good agreement with

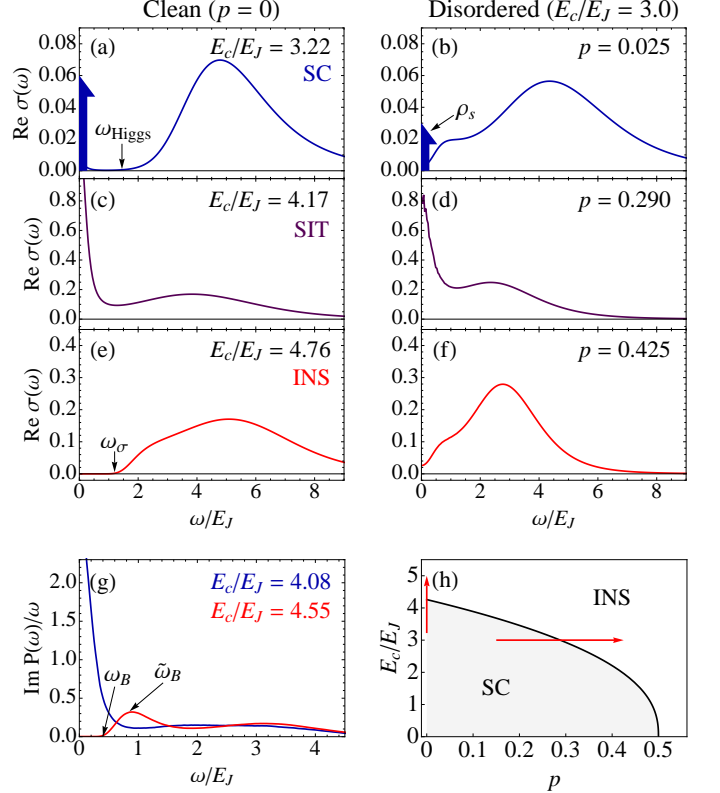


FIG. 3. (a-f): $\text{Re } \sigma(\omega)$ across the (a,c,e) clean ($p = 0$) and (b,d,f) disorder-tuned (fixed E_c/E_J) superconductor-insulator transitions. (g): Boson spectral function $\text{Im } P(\omega)/\omega$ for a clean superconducting (blue) and insulating (red) state. The energy scales shown in Fig. 2 are indicated in (a-g). In the disordered system, the spectral functions are marked by a significant increase in low frequency weight, obscuring the gap scales of the clean system. (h): Schematic phase diagram showing how the SIT can be crossed by either increasing E_c/E_J or by tuning the disorder p .

recent studies^{32–35} of the disorder-free problem.

Model: The quantum XY model is equivalent to a Josephson-junction array, with the Hamiltonian

$$\hat{H}_J = \frac{E_c}{2} \sum_i \hat{n}_i^2 - \sum_{\langle ij \rangle} J_{ij} \cos(\hat{\theta}_i - \hat{\theta}_j) \quad (1)$$

where the number operator \hat{n}_i at site i is canonically conjugate to the phase operator $\hat{\theta}_i$. Here E_c is the charging energy. The Josephson couplings are $J_{ij} = E_J$ with probability $(1 - p)$ and $J_{ij} = 0$ with probability p . The clean system ($p = 0$) is a coherent superconductor when E_J dominates over E_c , with phases aligned across all the junctions. However, large E_c/E_J favors a well-defined number eigenstate, leads to strong phase fluctuations, and drives the system into an insulating state. Thus E_c/E_J can be used to tune across the SIT in the clean system. A quantum phase transition can also be induced by increasing disorder p (bond dilution) for fixed E_c/E_J .

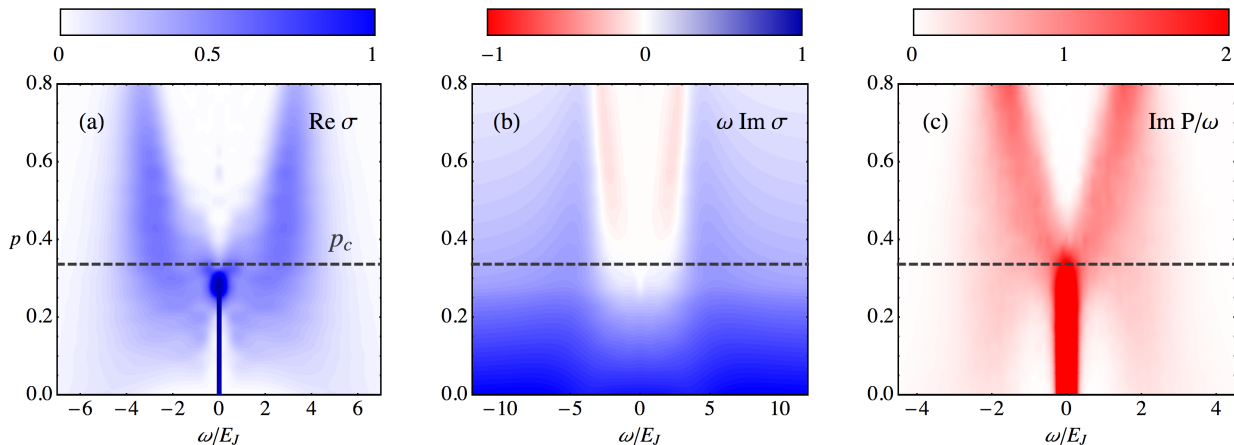


FIG. 4. Dynamical response functions across the disorder-tuned SIT. The critical disorder $p_c = 0.337$ is marked as a dashed line; $T/E_J = 0.156$ and $E_c/E_J = 3.0$. (a) In the conductivity $\text{Re } \sigma(\omega)$ the superfluid response is evident as a zero-frequency delta function of strength ρ_s . Deep in the insulator there is a gap in $\text{Re } \sigma(\omega)$ that grows with disorder. (b) $\omega \text{Im } \sigma(\omega)$ shows a crossover from “inductive” ($\omega \text{Im } \sigma(\omega) = \rho_s > 0$) to “capacitive” ($\omega \text{Im } \sigma(\omega) < 0$) behavior at small ω across the transition. (c) The boson spectral function $\text{Im } P(\omega)/\omega$, which has a peak centered about zero frequency in the superconductor, develops a characteristic scale $\tilde{\omega}_B$ in the insulator that grows with disorder.

(Fig. 3(h)). Thus Eq. 1 is a simple yet non-trivial model that describes a disorder-tuned SIT with a dynamical exponent $z = 1$.

Our results are obtained from calculations of the superfluid stiffness ρ_s , the complex conductivity $\sigma(\omega)$, and the boson spectral function $\text{Im } P(\omega)$. We estimate the superfluid stiffness ρ_s using $\rho_s/\pi = \Lambda_{xx}(q_x \rightarrow 0, q_y = 0, i\omega_n = 0) - \Lambda_{xx}(q_x = 0, q_y \rightarrow 0, i\omega_n = 0)$, which is the difference of the longitudinal and transverse pieces of the current-current correlation function Λ_{xx} . Here $j_x(\mathbf{r}, \tau) \sim \sin[\theta(\mathbf{r} + \hat{x}, \tau) - \theta(\mathbf{r}, \tau)]$ is the current and $\omega_n = 2\pi nT$ are Matsubara frequencies.

We use the Kubo formula for the complex conductivity $\sigma(\omega)$ expressed in terms of $\Lambda_{xx}(\mathbf{q} = 0, \tau)$ and transform the imaginary-time QMC results to real frequency using the maximum entropy method (MEM); see Methods. We have checked our results extensively using sum rules and compared the MEM results with direct estimates in imaginary time, as described in detail below. Similarly, we use QMC methods to calculate the imaginary time correlation function $P(\mathbf{r}, \tau) = \langle a^\dagger(\mathbf{r}, \tau) a(0, 0) \rangle$, where the bosonic creation operator is $a^\dagger = \exp i\theta(\mathbf{r}, \tau)$, and we obtain the spectral function $\text{Im } P(\omega)$ using the MEM.

Superconductor: We first discuss the SC and insulating state in both the clean and disordered systems, before turning to the quantum critical point. The SC state is characterized by a non-zero superfluid stiffness ρ_s (see Fig. 2). We use our calculated ρ_s to test the sum rule for the MEM-derived optical conductivity. The total spectral weight is given by $\int_0^\infty d\omega \text{Re } \sigma(\omega) = \pi \langle -k_x \rangle / 2$, where $\langle -k_x \rangle$ is the kinetic energy. We find that $\int_{0^+}^\infty d\omega \text{Re } \sigma(\omega)$ (note the lower limit of 0^+) calculated from the MEM result differs from $\langle -k_x \rangle$ by an amount that is exactly accounted for by the delta func-

tion $\rho_s \delta(\omega)$. We have checked this sum rule both in the clean and the disordered systems (see Supplementary Information).

In the clean superconductor (Fig. 3(a)), $\text{Re } \sigma(\omega)$ shows finite spectral weight above a threshold. Note that in the bosonic model, the cost of making electron-hole excitations is essentially infinite (i.e., much larger than all scales of interest). Phase fluctuations of the order parameter, $\Psi = A \exp(i\theta)$, lead to a current $\mathbf{j} \sim \text{Im } \Psi^* \nabla \Psi \sim |A|^2 \nabla \theta$. This then leads to the absorption threshold^{36,37} for creating a massive amplitude excitation (Higgs mode) and a massless phase excitation (phonon). Hence, we identify the threshold in $\text{Re } \sigma(\omega)$ with the Higgs scale ω_{Higgs} . We emphasize that even though the microscopic model (1) has only phase degrees of freedom, its long-wavelength behavior upon coarse-graining contains both amplitude (Higgs) and phase fluctuations (phonons and vortices). In addition, one can show that $\text{Re } \sigma(\omega)$ has a ω^5 tail at low energies arising from three-phonon absorption in a clean SC. The large power-law suppression, together with a very small numerical prefactor³⁸, however, makes this spectral weight too small to be visible in our numerical results for $\text{Re } \sigma(\omega)$.

As E_c/E_J is tuned to reach the SIT in the clean system, ρ_s decreases and vanishes at the transition; see Fig. 2. We also find that the Higgs scale goes soft upon approaching the quantum critical point, as expected.

The disordered SC results differ in several ways from those of the clean system. First, the superfluid stiffness ρ_s is reduced by disorder, vanishing at the SIT upon tuning the transition by disorder p . An important difference is the absence of a discernible Higgs threshold in $\text{Re } \sigma(\omega)$ for the disordered SC; see Fig. 3(b). Qualitatively we can understand this by the fact that once disorder breaks momentum conservation even single-phonon absorption is

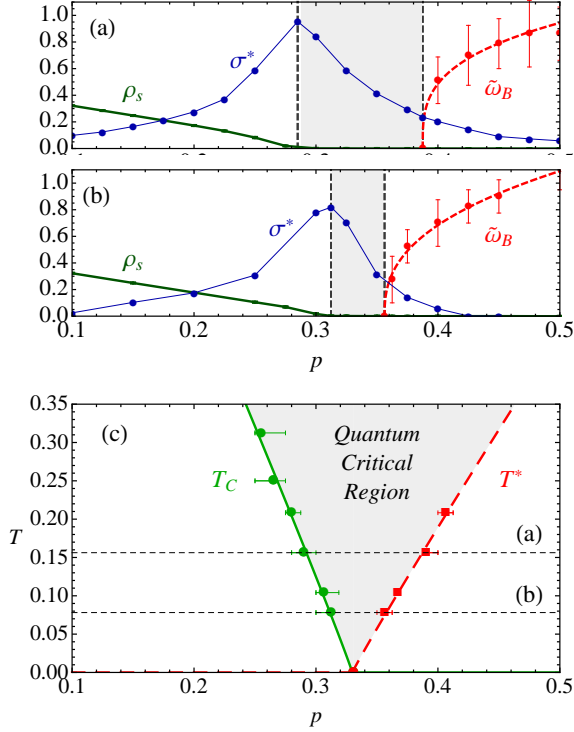


FIG. 5. (a,b) Superfluid stiffness ρ_s (green), bosonic scale $\tilde{\omega}_B$ (red) in the insulator, and low-frequency conductivity σ^* (blue), defined in the text, as functions of disorder p at two different temperatures shown in panel (c). The quantities are in units of E_J and $\sigma_Q = 4e^2/h$, respectively. The quantum critical region is shaded gray in all three panels. (c) Phase diagram with T_c determined by vanishing of ρ_s and T^* by the vanishing of $\tilde{\omega}_B$. The lines are fits to $|p-p_c|^{z\nu}$ with $p_c \approx 0.337$ and $z\nu \approx 0.96$.

permitted and one no longer needs a multi-phonon process for absorption. The effect of long-range Coulomb interactions, which change the phonon dispersion ($\sim q$) to that of a 2D plasmon ($\sim \sqrt{q}$), is an important open problem.

While the delta function in $\text{Re } \sigma(\omega)$ cannot be directly detected in dynamical experiments, its Kramers-Kronig transform in the reactive response $\text{Im } \sigma(\omega) = \rho_s/\omega$ can indeed be measured. In the SC, the finite low-frequency absorption in $\text{Re } \sigma(\omega)$ (due to the single-phonon processes discussed above) causes $\omega \text{Im } \sigma(\omega)$ to deviate from a constant, as is evident in Fig. 4. Our results are qualitatively similar to what has been seen in recent experiments, which, however, have focused on finite-temperature transitions in weakly disordered samples²⁰.

Insulator: The clean insulator shows a hard gap in $\text{Re } \sigma(\omega)$ with an absorption threshold that we denote by ω_σ ; see Fig. 3(e). To gain insight into this gap, we look at the boson spectral function $\text{Im } P(\omega)/\omega$ in Fig. 3(g), which too shows a hard gap ω_B , the analog of what was dubbed ω_{pair} in Ref. 10. The simplest process contributing to the conductivity is described diagrammatically as

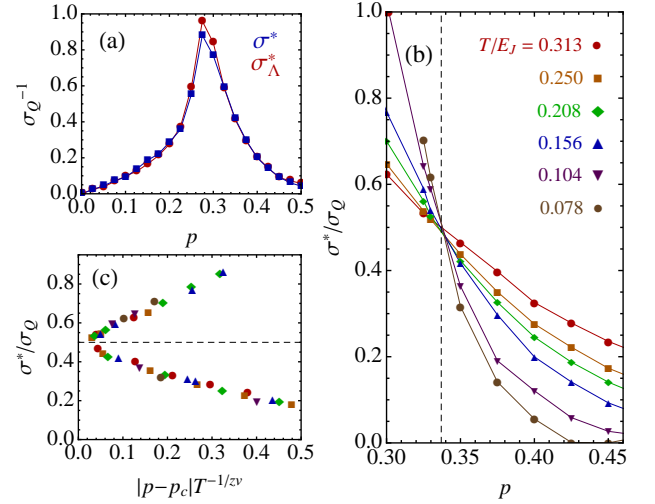


FIG. 6. (a) Comparison of two methods for obtaining the low-frequency conductivity near the SIT at $T/E_J = 0.156$, with σ^* from the integrated spectral weight in Eq. (2), and σ_Λ^* from the current correlator Λ_{xx} at imaginary time $\tau = \beta/2$ (see text). (b) Plot of $\sigma^*(T; p)$ as a function of the disorder p at various temperatures. The various curves cross at the critical disorder strength p_c at which σ^* is T -independent with the critical value $\sigma^* \approx 0.5\sigma_Q$. (c) Scaling collapse of the $\sigma^*(T; p)$ data with $p_c = 0.337$ and $z\nu = 0.96$, consistent with Fig. 5.

the convolution of two boson Greens functions leading to $\omega_\sigma = 2\omega_B$ as seen in Fig. 2. We also see that both of these energy scales go soft as the SIT is approached from the insulating side. In addition, there is a well-defined peak in $\text{Im } P(\omega)/\omega$ at a characteristic scale $\tilde{\omega}_B$ in the boson spectral function $\text{Im } P(\omega)/\omega$, whose evolution with disorder is most readily seen in the “slingshot-like” plot in Fig. 4(c). The corresponding changes in $\text{Re } \sigma(\omega)$ are shown in Fig. 4(a). We also note that there is a marked change in $\text{Im } \sigma(\omega)$ across the SIT. We see from Fig. 4(b) that it changes sign at low frequencies from an inductive ($\text{Im } \sigma(\omega) > 0$) to a capacitive ($\text{Im } \sigma(\omega) < 0$) response going through the disorder-tuned SIT.

In contrast to the hard gap of the clean system, the dirty insulator exhibits absorption down to arbitrarily low frequencies (see Fig. 3(f)), which is, at least in part, due to rare regions. This then raises the question: what is the characteristic energy scale that goes soft as one approaches the SIT from the insulating side? We find that this scale is the location of the low-energy peak at $\tilde{\omega}_B$ in the boson spectral function $\text{Im } P(\omega)/\omega$, whose evolution with disorder is most readily seen in the “slingshot-like” plot in Fig. 4(c). The corresponding changes in $\text{Re } \sigma(\omega)$ are shown in Fig. 4(a). We also note that there is a marked change in $\text{Im } \sigma(\omega)$ across the SIT. We see from Fig. 4(b) that it changes sign at low frequencies from an inductive ($\text{Im } \sigma(\omega) > 0$) to a capacitive ($\text{Im } \sigma(\omega) < 0$) response going through the disorder-tuned SIT.

Quantum criticality: We have already discussed the various scales that go soft on approaching the SIT from either side. The results for the clean system, with SIT tuned by E_c/E_J , are summarized in Fig. 2. We now analyze the results for the disordered system. The finite temperature QMC data, taken at face value, suggest a finite separation between the disorder values at which ρ_s goes to zero from the SC side and the characteristic boson scale $\tilde{\omega}_B$ vanishes from the insulating side; see Fig. 5

(a,b). We emphasize that this intermediate region is *not* a *Bose metal* separating the SC and insulator, but rather the quantum critical region. As shown in Fig. 5 (c), the SC transition temperature T_c , at which ρ_s vanishes, and the crossover scale T^* , at which $\tilde{\omega}_B$ vanishes, define this fan-shaped critical region. (We have used $z = 1$ in scaling the system size as we go down in temperature in Fig. 5 (c).) Both T_c and T^* extrapolate to zero at the same critical disorder $p_c \approx 0.337$ (for the chosen value of E_c/E_J) with the scaling $|p - p_c|^{z\nu}$ where $z = 1$ and $\nu = 0.96 \pm 0.06$.

Finally, we turn to the important question of the universal conductivity at the SIT^{29–32,39}. The d.c. limit requires $\omega \rightarrow 0$ first and then $T \rightarrow 0$, which is not possible when analytically continuing Matsubara data⁴⁰. What we can meaningfully do is to exploit quantum critical scaling and sum rules. The MEM results (i) satisfy the conductivity sum rule, which integrates over all frequencies (see Methods), and (ii) are reliable for high frequencies $\omega > 2\pi T$. Taking the difference of integrated spectral weights, we can reliably estimate $\sigma^* = (2\pi T)^{-1} \int_{0+}^{2\pi T} d\omega \text{Re} \sigma(\omega, T; p)$. We may now use the universal scaling form⁴⁰ $\text{Re} \sigma(\omega, T; p) = \sigma_Q \Phi(\omega/T; |p - p_c| T^{-1/z\nu})$, with $\sigma_Q = 4e^2/h$, to obtain

$$\sigma^*(T; p) = \frac{\sigma_Q}{2\pi} \int_{0+}^{2\pi} dx \Phi(x; |p - p_c| T^{-1/z\nu}). \quad (2)$$

Thus σ^* is a T -independent universal constant at the quantum critical point $p = p_c$ and closely related to the low frequency conductivity measured in experiments.

Another estimate of the low-frequency conductivity comes directly from the current correlator $\sigma_A^* = \beta^2 \Lambda_{xx}(\mathbf{q} = 0, \tau = \beta/2)/\pi$ at the largest available value of imaginary time⁴¹. The σ^* estimates obtained by the two methods show good agreement (Fig. 6(a)) and provide a non-trivial check on the analytic continuation.

In Fig. 6 (b) we plot $\sigma^*(T; p)$ as a function of p for various temperatures. In the superconductor ($p < p_c$) the conductivity increases with decreasing T , while the opposite trend is observed in the insulator ($p > p_c$). Precisely at the SIT $p = p_c$, we find a T -independent crossing point which also allows us to estimate the critical σ^* . Another way to scale the data is to plot $\sigma^*(T; p)$ as a function of the scaling variable $|p - p_c| T^{-1/z\nu}$. We find data collapse for $p_c = 0.337$ and $z\nu = 0.96$ (consistent with Fig. 5) with a critical value of $\sigma^* \approx 0.5\sigma_Q$. For a detailed comparison of the critical exponents and σ^* with previous results⁴², see the Supplemental Information.

Conclusions: We have presented calculations of the complex dynamical conductivity $\sigma(\omega)$ and the boson spectral function $P(\omega)$ across the SIT driven by increasing the charging energy E_c/E_J as well as by increasing disorder p . By comparison of the clean and disordered problems, we see the effect of disorder on the Higgs scale ω_{Higgs} in the superconductor and on the threshold ω_σ in the insulator, in generating low frequency weight in absorption in both superconducting and insulating phases,

and in expanding the region over which critical fluctuations are observable. It is important to emphasize that the effects we have calculated have required going beyond mean field theories, even those that included emergent granularity due to the microscopic disorder, by focussing on the role of fluctuations of the order parameter. We have calculated the effect of these fluctuations, both amplitude and phase, on experimentally accessible observables using QMC methods coupled with maximum entropy methods, constrained by sum rules. Recently the AdS-CFT holographic mapping has been used to obtain the dynamical conductivity at the disorder-free bosonic quantum critical point^{34,35}. Our focus here has been on the evolution of the dynamical quantities in both the phases, superconducting and insulating, and across the disorder-driven SIT, for which the holographic formalism has not yet been developed.

Our calculations have laid the foundation for key signatures in dynamical response functions across quantum phase transitions. Though we have focused on the disorder-driven s-wave SIT in thin films, the ideas are equally relevant for a diverse set of problems, including: (i) unconventional superconductors like the high T_c cuprates that have a quantum critical point tuned by doping, (ii) SIT at oxide interfaces like $\text{LaAlO}_3/\text{SrTiO}_3$, (iii) SIT in the next generation of weakly coupled layered materials like dichalcogenide monolayers, and (iv) bosons in optical lattices with speckle disorder.

Acknowledgements: We thank Assa Auerbach and Subir Sachdev for discussions. M.R. and N.T. acknowledge the hospitality of the Aspen Center for Physics, supported in part by NSF PHYS-1066293. We gratefully acknowledge support from an NSF Graduate Research Fellowship (M.S.), DOE DE-FG02-07ER46423 (N.T.), NSF DMR-1006532 (M.R.), and computational support from the Ohio Supercomputing Center.

Methods

Monte Carlo simulations: We analyze the (2+1)D quantum XY model by mapping it onto an anisotropic 3D classical XY model with Hamiltonian³¹

$$H_{\text{XY}} = -K_\tau \sum_{\mathbf{r}, j} \cos[\theta_{\mathbf{r}}(\tau_j) - \theta_{\mathbf{r}}(\tau_{j+1})] - K_0 \sum_{\langle \mathbf{r}, \mathbf{r}' \rangle, j} \cos[\theta_{\mathbf{r}}(\tau_j) - \theta_{\mathbf{r}'}(\tau_j)] \quad (3)$$

by performing a Trotter decomposition of imaginary time into L_τ slices of width $\Delta\tau$ such that the inverse temperature $\beta = L_\tau \Delta\tau$; \mathbf{r} and \mathbf{r}' are points in the 2D plane and τ_j denotes the j^{th} imaginary time slice; and the dimensionless coupling constants are $K_\tau = 1/\Delta\tau E_c$ and $K_0 = \Delta\tau E_J$.

We perform Monte Carlo simulations using the efficient Wolff cluster update method⁴³. In all of our simulations, we have set $K_0 = 0.1$, which we have checked to be sufficiently small to remove the error from the Trotter decomposition. For the clean system, we performed simulations

on lattices of size 256×256 with $L_\tau = 64$. For the disorder tuned transition, we worked at fixed $E_c/E_J = 3.0$. Simulations at different temperatures have been performed by changing the number of imaginary time slices L_τ from 32 to 128; for each L_τ , we fix $L = L_\tau$ since the dynamical exponent is $z = 1$. All disorder results have been averaged over 100 disorder realizations.

Dynamical observables: We calculate the imaginary time, or equivalently the Matsubara frequency ($\omega_n = 2n\pi/\beta$), current-current correlation function

$$\Lambda_{xx}(\mathbf{q}; i\omega_n) = \sum_{\mathbf{r}} \int_0^\beta d\tau \langle j_x(\mathbf{r}, \tau) j_x(0, 0) \rangle e^{i\mathbf{q} \cdot \mathbf{r}} e^{-i\omega_n \tau} \quad (4)$$

where the paramagnetic current in our model is given by $j_x(\mathbf{r}, \tau) \equiv K_0 \sin[\theta(\mathbf{r} + \hat{x}, \tau) - \theta(\mathbf{r}, \tau)]$. The conductivity is related to the analytic continuation of Λ_{xx} at $\mathbf{q} = 0$

$$\sigma(\omega) = [\langle -k_x \rangle - \Lambda_{xx}(\omega + i0^+)] / i(\omega + i0^+) \quad (5)$$

where $\langle -k_x \rangle$ is the average kinetic energy along bonds in the x -direction. $\text{Re } \sigma(\omega)$ is then given by

$$\text{Re } \sigma(\omega) = \rho_s \delta(\omega) + \text{Im } \Lambda_{xx}(\omega) / \omega. \quad (6)$$

The superfluid stiffness ρ_s is obtained from the difference between the transverse and longitudinal limits of the current-current correlation function $\rho_s/\pi = \Lambda_{xx}(q_x \rightarrow 0, q_y = 0, i\omega_n = 0) - \Lambda_{xx}(q_x = 0, q_y \rightarrow 0, i\omega_n = 0)$ and

the sum rule $\langle -k_x \rangle = \Lambda_{xx}(q_x \rightarrow 0, q_y = 0, i\omega_n = 0)$. Finally, $\text{Re } \sigma(\omega)$ obeys the optical conductivity sum rule $2 \int_0^\infty d\omega \text{Re } \sigma(\omega) = \pi \langle -k_x \rangle - \rho_s$, which serves as a non-trivial check on our analytic continuation results.

The boson spectral function is obtained from the analytical continuation of the bosonic Greens function $P(\tau) = L^{-2} \sum_{\mathbf{r}} \langle a^\dagger(\mathbf{r}, \tau) a(\mathbf{r}, 0) \rangle$, with $a^\dagger(\mathbf{r}, \tau) = \exp\{i\theta(\mathbf{r}, \tau)\}$. The spectral function $P(\omega)$ obeys the following two sum rules $\int_{-\infty}^\infty d\omega / \pi \text{Im } P(\omega) / [1 - e^{-\beta\omega}] = 1$ and $\int_{-\infty}^\infty d\omega / \pi \text{Im } P(\omega) / \omega = \int_0^\beta d\tau P(\tau)$.

Analytic continuation: The imaginary time correlator $\Lambda_{xx}(\tau)$ calculated in our Monte Carlo simulations is related to its real-frequency counterpart through

$$\Lambda_{xx}(\tau) = \int_{-\infty}^\infty \frac{d\omega}{\pi} \frac{e^{-\omega\tau}}{1 - e^{-\beta\omega}} \text{Im } \Lambda_{xx}(\omega). \quad (7)$$

To extract the boson spectral function, we have an expression very similar to eq. (7) with $\Lambda_{xx}(\tau) \rightarrow P(\tau)$ on the left hand side and $\text{Im } \Lambda_{xx}(\omega) \rightarrow \text{Im } P(\omega)$ on the right.

To extract real frequency information, we have employed the maximum entropy method (MEM)⁴⁴ to invert this Laplace transform. We have performed extensive tests on our Maximum Entropy routine, and checked that all of the resulting ω -dependent functions obey the sum rules described above; see Supplementary Information for more details.

-
- ¹ Hebard, A. F. & Paalanen, M. A. Magnetic-field-tuned superconductor-insulator transition in two-dimensional films. *Phys. Rev. Lett.* **65**, 927–930 (1990).
 - ² Shahar, D. & Ovadyahu, Z. Superconductivity near the mobility edge. *Phys. Rev. B* **46**, 10917–10922 (1992).
 - ³ Adams, P. Field-Induced Spin Mixing in Ultra-Thin Superconducting Al and Be Films in High Parallel Magnetic Fields. *Phys. Rev. Lett.* **92**, 067003 (2004).
 - ⁴ Sambandamurthy, G., Engel, L. W., Johansson, A. & Shahar, D. Superconductivity-Related Insulating Behavior. *Phys. Rev. Lett.* **92**, 107005 (2004).
 - ⁵ Steiner, M. A., Boebinger, G. & Kapitulnik, A. Possible Field-Tuned Superconductor-Insulator Transition in High- T_c Superconductors: Implications for Pairing at High Magnetic Fields. *Phys. Rev. Lett.* **94**, 107008 (2005).
 - ⁶ Stewart, M. D., Yin, A., Xu, J. M. & Valles, J. M. Superconducting Pair Correlations in an Amorphous Insulating Nanohoneycomb Film. *Science* **318**, 1273 (2007).
 - ⁷ Gantmakher, V. F. & Dolgoplov, V. T. Superconductor-insulator quantum phase transition. *Physics-Uspekhi* **53**, 3 (2010).
 - ⁸ Ghosal, A., Randeria, M. & Trivedi, N. Role of Spatial Amplitude Fluctuations in Highly Disordered s-Wave Superconductors. *Phys. Rev. Lett.* **81**, 3940 (1998).
 - ⁹ Ghosal, A., Randeria, M. & Trivedi, N. Inhomogeneous pairing in highly disordered s-wave superconductors. *Phys. Rev. B* **65**, 014501 (2001).
 - ¹⁰ Bouadim, K., Loh, Y. L., Randeria, M. & Trivedi, N.

- Single- and two-particle energy gaps across the disorder-driven superconductor-insulator transition. *Nat Phys* **7**, 884–889 (2011).
- ¹¹ Sacépé, B., Chapelier, C., Baturina, T. I., Vinokur, V. M., Baklanov, M. R. & Sanquer, M. Pseudogap in a thin film of a conventional superconductor. *Nature Communications* **1**, 140 (2010).
- ¹² Sacépé, B., Dubouchet, T., Chapelier, C., Sanquer, M., Ovadia, M., Shahar, D., Feigel'man, M. & Ioffe, L. Localization of preformed Cooper pairs in disordered superconductors. *Nat. Phys.* **7**, 239–244 (2011).
- ¹³ Mondal, M., Kamlapure, A., Chand, M., Saraswat, G., Kumar, S., Jesudasan, J., Benfatto, L., Tripathi, V. & Raychaudhuri, P. Phase Fluctuations in a Strongly Disordered s-Wave NbN Superconductor Close to the Metal-Insulator Transition. *Phys. Rev. Lett.* **106**, 047001 (2011).
- ¹⁴ Sherman, D., Kopnov, G., Shahar, D. & Frydman, A. Measurement of a Superconducting Energy Gap in a Homogeneously Amorphous Insulator. *Phys. Rev. Lett.* **108**, 177006 (2012).
- ¹⁵ Crane, R. W., Armitage, N. P., Johansson, A., Sambandamurthy, G., Shahar, D. & Grüner, G. Fluctuations, dissipation, and nonuniversal superfluid jumps in two-dimensional superconductors. *Phys. Rev. B* **75**, 094506 (2007).
- ¹⁶ Crane, R., Armitage, N. P., Johansson, A., Sambandamurthy, G., Shahar, D. & Grüner, G. Survival of superconducting correlations across the two-dimensional

- superconductor-insulator transition: A finite-frequency study. *Phys. Rev. B* **75**, 184530 (2007).
- ¹⁷ Liu, W., Kim, M., Sambandamurthy, G. & Armitage, N. P. Dynamical study of phase fluctuations and their critical slowing down in amorphous superconducting films. *Phys. Rev. B* **84**, 024511 (2011).
 - ¹⁸ Liu, W., Pan, L., Wen, J., Kim, M., Sambandamurthy, G. & Armitage, N. P. Microwave Spectroscopy Evidence of Superconducting Pairing in the Magnetic-Field-Induced Metallic State of InO_x Films at Zero Temperature. *Phys. Rev. Lett.* **111**, 067003 (2013).
 - ¹⁹ Lemarié, G., Kamlapure, A., Bucheli, D., Benfatto, L., Lorenzana, J., Seibold, G., Ganguli, S. C., Raychaudhuri, P. & Castellani, C. Universal scaling of the order-parameter distribution in strongly disordered superconductors. *Phys. Rev. B* **87**, 184509 (2013).
 - ²⁰ Mondal, M., Kamlapure, A., Ganguli, S. C., Jesudasan, J., Bagwe, V., Benfatto, L. & Raychaudhuri, P. Enhancement of the finite-frequency superfluid response in the pseudogap regime of strongly disordered superconducting films. *Sci. Rep.* **3**, 1357 (2013).
 - ²¹ Fisher, M. P. A., Weichman, P. B., Grinstein, G. & Fisher, D. S. Boson localization and the superfluid-insulator transition. *Phys. Rev. B* **40**, 546–570 (1989).
 - ²² Jaksch, D., Bruder, C., Cirac, J. I., Gardiner, C. W. & Zoller, P. Cold Bosonic Atoms in Optical Lattices. *Phys. Rev. Lett.* **81**, 3108–3111 (1998).
 - ²³ Greiner, M., Mandel, O., Esslinger, T., Hansch, T. W. & Bloch, I. Quantum phase transition from a superfluid to a Mott insulator in a gas of ultracold atoms. *Nature* **415**, 39–44 (2002).
 - ²⁴ Spielman, I. B., Phillips, W. D. & Porto, J. V. Mott-Insulator Transition in a Two-Dimensional Atomic Bose Gas. *Phys. Rev. Lett.* **98**, 080404 (2007).
 - ²⁵ Gurarie, V., Pollet, L., Prokof'ev, N. V., Svistunov, B. V. & Troyer, M. Phase diagram of the disordered Bose-Hubbard model. *Phys. Rev. B* **80**, 214519 (2009).
 - ²⁶ Billy, J., Josse, V., Zuo, Z., Bernard, A., Hambrecht, B., Lugan, P., Clement, D., Sanchez-Palencia, L., Bouyer, P. & Aspect, A. Direct observation of Anderson localization of matter waves in a controlled disorder. *Nature* **453**, 891–894 (2008).
 - ²⁷ Kondov, S. S., McGehee, W. R., Zirbel, J. J. & DeMarco, B. Three-Dimensional Anderson Localization of Ultracold Matter. *Science* **334**, 66–68 (2011).
 - ²⁸ Kondov, S. S., McGehee, W. R. & DeMarco, B. Interplay of disorder and interactions in an optical lattice Hubbard model. *ArXiv e-prints 1305.6072* (2013).
 - ²⁹ Cha, M.-C., Fisher, M. P. A., Girvin, S. M., Wallin, M. & Young, A. P. Universal conductivity of two-dimensional films at the superconductor-insulator transition. *Phys. Rev. B* **44**, 6883–6902 (1991).
 - ³⁰ Sørensen, E. S., Wallin, M., Girvin, S. M. & Young, A. P. Universal conductivity of dirty bosons at the superconductor-insulator transition. *Phys. Rev. Lett.* **69**, 828–831 (1992).
 - ³¹ Cha, M.-C. & Girvin, S. M. Universal conductivity in the boson Hubbard model in a magnetic field. *Phys. Rev. B* **49**, 9794–9801 (1994).
 - ³² Šmakov, J. & Sørensen, E. Universal Scaling of the Conductivity at the Superfluid-Insulator Phase Transition. *Phys. Rev. Lett.* **95**, 180603 (2005).
 - ³³ Gazit, S., Podolsky, D., Auerbach, A. & Arovas, D. P. Dynamics and Conductivity Near Quantum Criticality. *ArXiv e-prints 1309.1765* (2013).
 - ³⁴ Witczak-Krempa, W., Sorensen, E. & Sachdev, S. The dynamics of quantum criticality: Quantum Monte Carlo and holography. *ArXiv e-prints 1309.2941* (2013).
 - ³⁵ Chen, K., Liu, L., Deng, Y., Pollet, L. & Prokof'ev, N. Universal Conductivity in a Two-dimensional Superfluid-to-Insulator Quantum Critical System. *ArXiv e-prints 1309.5635* (2013).
 - ³⁶ Lindner, N. H. & Auerbach, A. Conductivity of hard core bosons: A paradigm of a bad metal. *Phys. Rev. B* **81**, 054512 (2010).
 - ³⁷ Gazit, S., Podolsky, D. & Auerbach, A. Fate of the Higgs Mode Near Quantum Criticality. *Phys. Rev. Lett.* **110**, 140401 (2013).
 - ³⁸ Podolsky, D., Auerbach, A. & Arovas, D. P. Visibility of the amplitude (Higgs) mode in condensed matter. *Phys. Rev. B* **84**, 174522 (2011).
 - ³⁹ Lin, F., Sørensen, E. S. & Ceperley, D. M. Superfluid-insulator transition in the disordered two-dimensional Bose-Hubbard model. *Phys. Rev. B* **84**, 094507 (2011).
 - ⁴⁰ Damle, K. & Sachdev, S. Nonzero-temperature transport near quantum critical points. *Phys. Rev. B* **56**, 8714–8733 (1997).
 - ⁴¹ Trivedi, N., Scalettar, R. T. & Randeria, M. Superconductor-insulator transition in a disordered electronic system. *Phys. Rev. B* **54**, R3756 (1996).
 - ⁴² Iyer, S., Pekker, D. & Refael, G. Mott glass to superfluid transition for random bosons in two dimensions. *Phys. Rev. B* **85**, 094202 (2012).
 - ⁴³ Wolff, U. Collective Monte Carlo Updating for Spin Systems. *Phys. Rev. Lett.* **62**, 361–364 (1989).
 - ⁴⁴ Gubernatis, J. E., Jarrell, M., Silver, R. N. & Sivia, D. S. Quantum Monte Carlo simulations and maximum entropy: Dynamics from imaginary-time data. *Phys. Rev. B* **44**, 6011–6029 (1991).